Journal of Marine Research, 55, 93–115, 1997

Large-scale processes in the upper layers of the Indian Ocean inferred from temperature climatology

by A. S. Unnikrishnan[1], S. Prasanna Kumar[1] and G. S. Navelkar[1]

ABSTRACT

Determination of amplitudes and phases for the annual and semi-annual cycle of the temperature in the Indian Ocean north of 20S from Levitus temperature climatology (1982) gives maximum amplitudes of the seasonal cycle at 100 m with the dominance of semi-annual cycle in the equatorial region and annual cycle elsewhere in the domain. The Bay of Bengal shows characteristics of the westward-propagating Rossby waves of annual period, while the Arabian Sea shows the dominance of Ekman pumping in the central region and westward-propagating features in the eastern region. Qualitative evidences obtained from the distribution of depth of 20°C isotherm and computed Ekman pumping velocities are consistent with the above inferences. From the time-longitude plot of the depth of the 20°C isotherm, the phase speed of westward propagating features from the west coast of India along 10.5N and 15.5N are found to be 7.8 cm s^{-1} and 5.2 cm s^{-1} respectively. This is consistent with the corresponding values computed and verified with theory for the Bay of Bengal (Prasanna Kumar and Unnikrishnan, 1995).

1. Introduction

One of the characteristic features of the Indian Ocean north of 20S is the variability associated with the monsoonal wind reversals. Studies on the Indian Ocean dynamics and large-scale processes are limited due to paucity of data. The major references for the Indian Ocean research, except in the Somali and Madagascar region (e.g., Bruce *et al.,* 1980; Lutjeharms *et al.,* 1981; Quadfasel and Schott, 1982, 1983; Grundlingh, 1985; Swallow *et al.,* 1988; Schott *et al.,* 1990), still remain the atlas of Wyrtki (1971) prepared based on the International Indian Ocean Expedition data and that of Cutler and Swallow (1984) using the ship drift data collected by the British meteorological office. Rao *et al.* (1989) described the SST and mixed layer variability in the Indian Ocean using historical data. Some of the recent studies suggest the existence of semi-annual periodicities due to semi-annual reversal of wind (Gent *et al.,* 1983; Clarke and Liu, 1993). However, it is not fully known which are the regions in the Indian Ocean that really exhibit semi-annual variability.

In the present paper, we address mainly two questions regarding the large-scale processes in the upper layers of the Indian Ocean: (1) which are the regions that respond to dominant semi-annual and annual variability and (2) what are the relative roles of local

1. National Institute of Oceanography, Dona Paula, Goa 403 004, India.

forcing and remote forcing in various regions, particularly in the northern Indian Ocean? We accomplish this by looking into the seasonal variabilities in the upper layers using the climatological temperature data of Levitus (1982). Earlier, we made a similar analysis (Prasanna Kumar and Unnikrishnan, 1995) for the Bay of Bengal region, between 80 and 100E, which was mainly intended to study the characteristics of westward propagating Rossby waves in the Bay of Bengal. In the present work, we have extended the analysis to the entire region north of 20S in the Indian Ocean. First, we determine amplitudes and phases of the annual and semi-annual cycles of temperature, wind stress components and curl of the wind stress. Second, the relative roles of Ekman pumping and remote forcing in the dynamics of the northern Indian Ocean are studied, based on the distribution of depth of 20°C isotherm along various latitude sections and the distribution of computed Ekman pumping velocities. We also attempt to bring out the relative dominance of semi-annual and annual periodicities in different regions of the Indian Ocean.

2. Method

The monthly mean temperature data of Levitus (1982), for each one degree square is subjected to a least squares analysis similar to that described in Wyrtki (1965). The observed temperature can be written as $T = T_0 + T_1 \cos(\omega t - \Phi_1) + T_2 \cos(2\omega t - \Phi_2)$, where T_1 and Φ_1 are the amplitude and phase of the annual cycle; T_2 and Φ_2 are the corresponding parameters for the semi-annual cycle, T_0 is the average value and ω is the frequency corresponding to one year. A least square fit is performed between the above function of temperature and the observed temperature to obtain the amplitudes and phases of annual and semi-annual periods. The analysis is carried out for each one degree square for a domain north of 20S between 40 and 120E longitudes in the Indian Ocean.

3. Results

a. Amplitude and phase distribution of the seasonal cycle of temperature

i. Annual cycle. Amplitudes and phases of the annual cycle of temperature at 10, 100 and 200 m depths are shown in Figures 1 to 3. Note that the phases vary from −180° to 180°, with 30° corresponding to one month. The amplitude distribution at 10 m (Fig. 1a) shows low values of less than 0.5°C in the equatorial region, which increase gradually away from the equator and reach upto 2.5°C near 20N and 20S. This is similar to the features in the charts of the amplitudes of SST, for the North Pacific, presented by Wyrtki (1965). Effects of monsoonal variabilities are not evident in these figures, but they are found in the semi-annual amplitudes (Fig. 4a). The phase distribution (Fig. 1b) shows a northward increase, coinciding with the solar insolation maximum, with the temperature maximum occurring between March and May. Note that the phases are with respect to the middle of January.

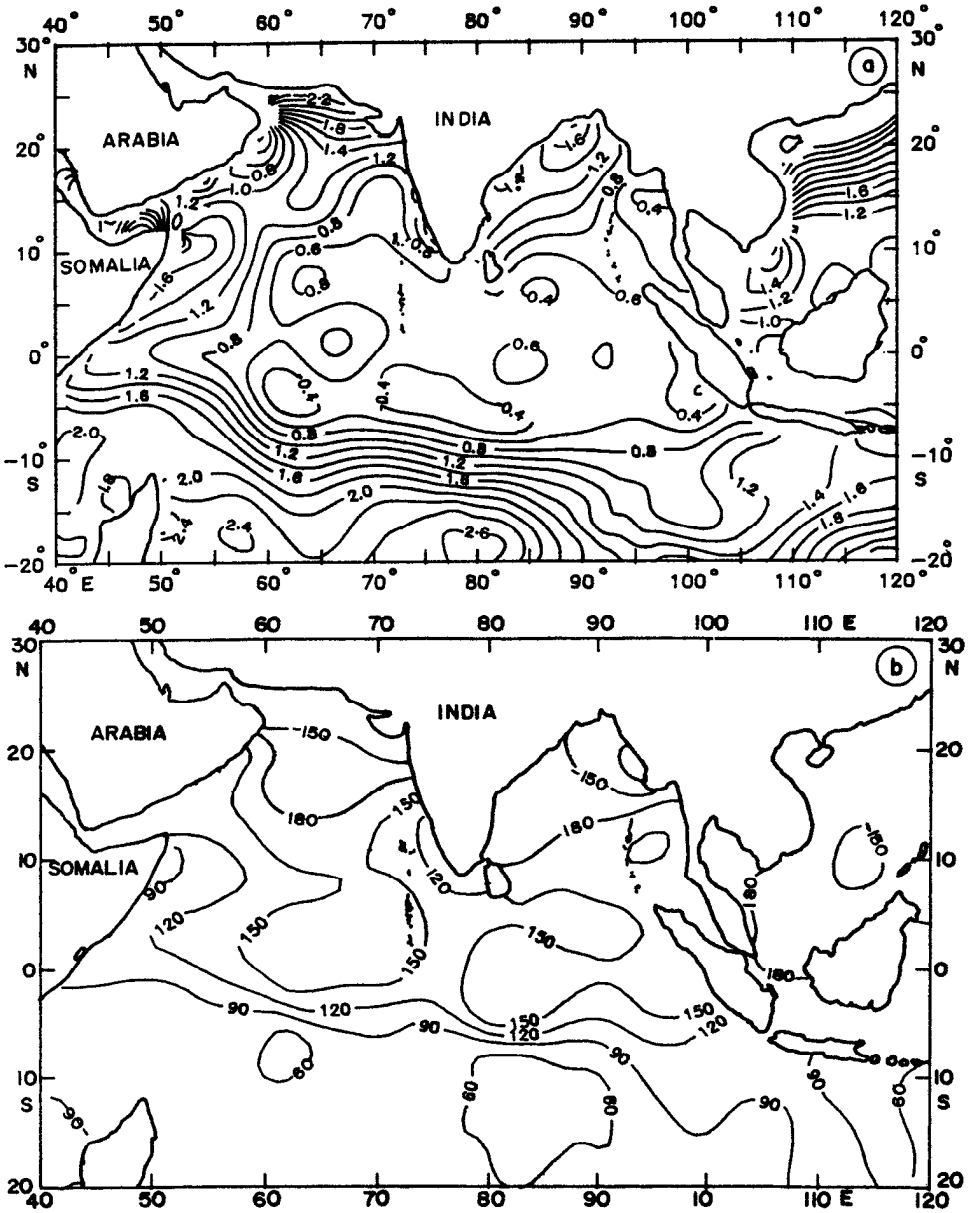

Figure 1. The distribution of (a) amplitude (°C) and (b) Phase (deg.) of seasonal cycle of temperature at 10 m for annual periodicity. Note that the phase values range from −180 to 180 degrees with 0 degree corresponding to the middle of January.

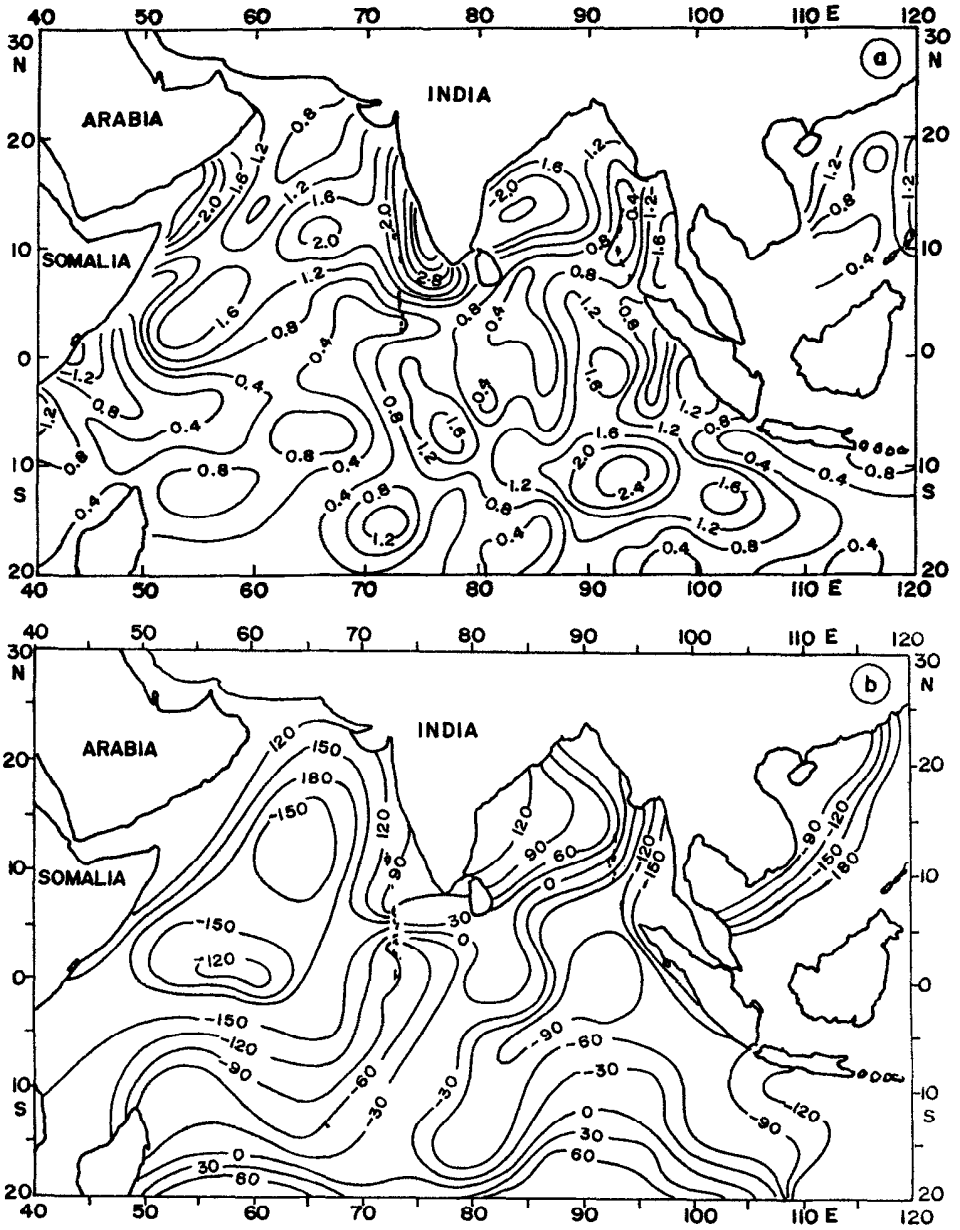

Figure 2. The distribution of (a) amplitude (°C) and (b) phase (deg.) of seasonal cycle of temperature at 100 m for annual periodicity. Note that the phase values range from −180 to 180 degrees with 0 degree corresponding to the middle of January.

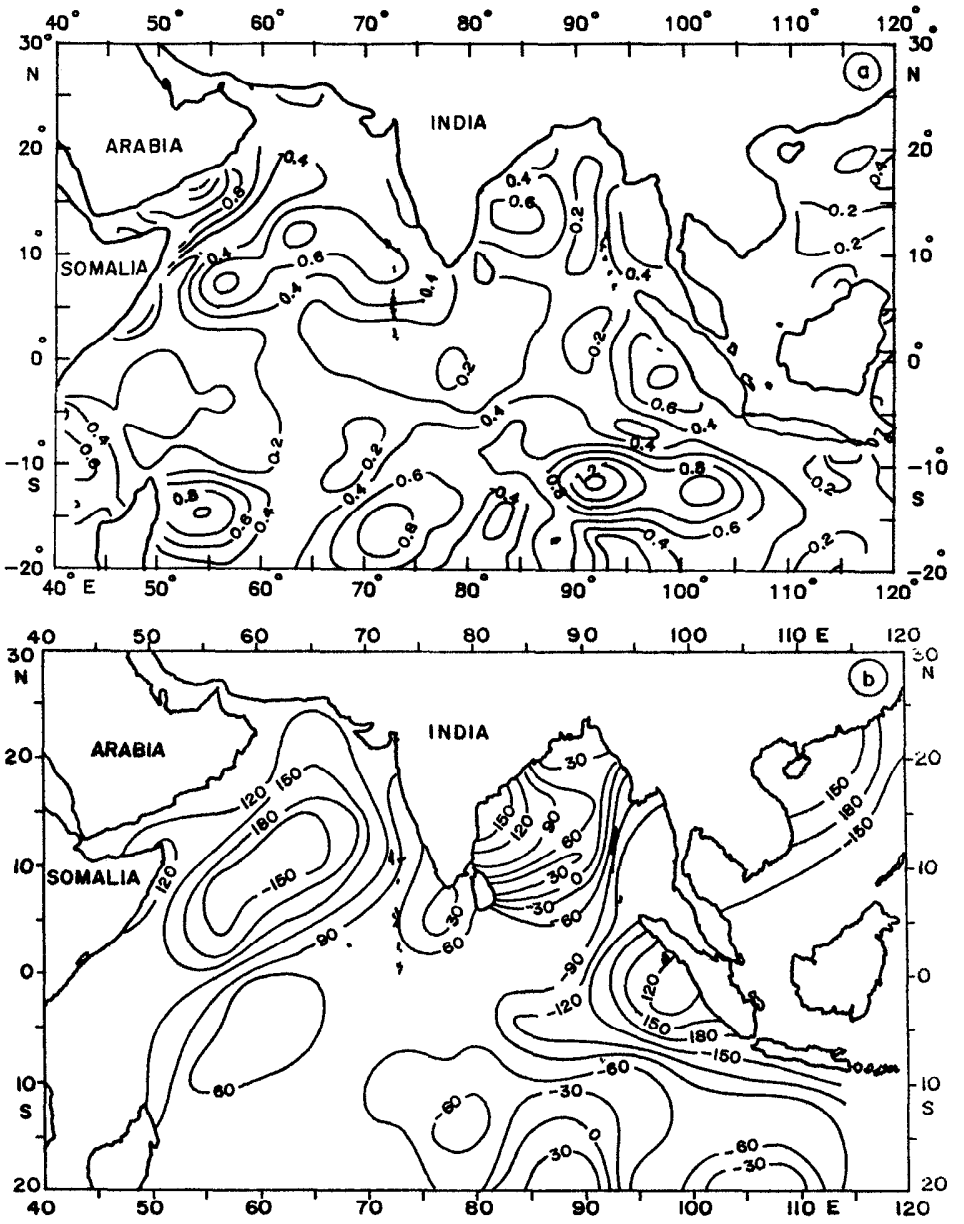

Figure 3. The distribution of (a) amplitude (°C) and (b) phase (deg.) of seasonal cycle of temperature at 200 m for annual periodicity. Note that the phase values range from −180 to 180 degrees with 0 degree corresponding to the middle of January.

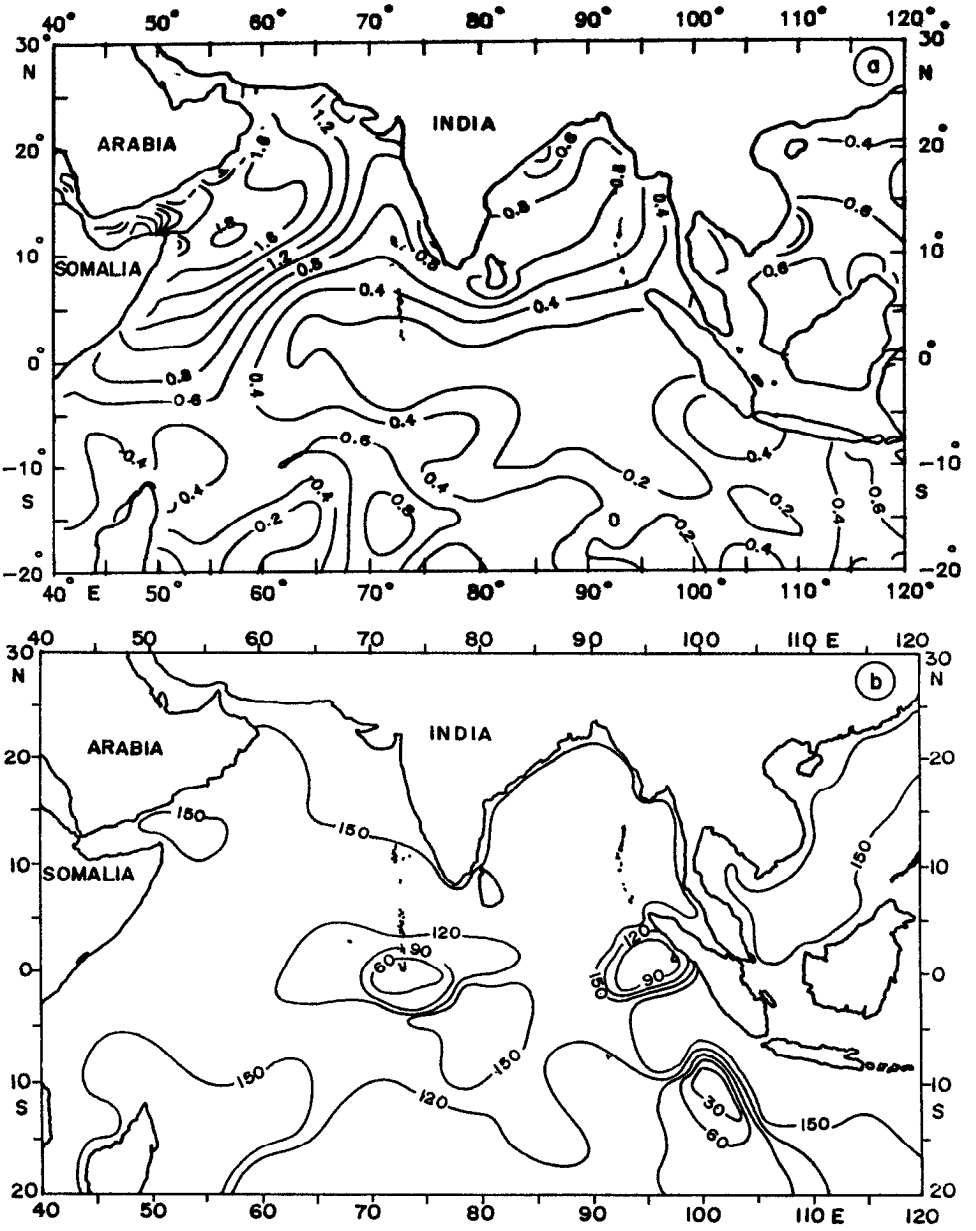

Figure 4. The distribution of (a) amplitude (°C) and (b) phase (deg.) of seasonal cycle of temperature at 10 m for the semi-annual periodicity. Note that the phase values range from 0 to 180 degrees.

At 100 m (Fig. 2a), the amplitude distribution pattern is quite different from that of the near-surface layer. High amplitudes of greater than 2.0°C are found in the western part of the Bay of Bengal and in the eastern Arabian Sea. Remarkably high amplitudes off the southwest coast of India are found and the isolines protrude southward as a tongue-like

feature. South of the equator, the pattern of highs and lows is organized and oriented in a zonal direction. The phase distribution at 100 m depth (Fig. 2b) also differs from that at the surface. There is no characteristic pattern south of the equator. In the Bay of Bengal, the westward increase in the phase values are due to the westward-propagating Rossby waves (Prasanna Kumar and Unnikrishnan, 1995). A similar feature is not clearly noticeable in the Arabian Sea; however, a subsequent analysis based on the depth of 20°C isotherm does reveal signatures of westward propagation in the eastern Arabian Sea as well. In the central Arabian Sea, there is a large region of uniform phase. Across the western coasts of the north Indian Ocean and the coast of India, large phase differences indicate large zonal temperature gradients.

At 200 m depth (Fig. 3a), the amplitudes are lower (maximum of about 1.2°C) than those at 100 m. But the pattern is similar to that at 100 m, except for the absence of high amplitudes along the southwest coast of India. The phase distribution at 200 m (Fig. 3b) is nearly the same as that at 100 m. At 300 m, the amplitudes are very small (not presented) and the seasonal variations can be considered insignificant below this depth.

ii. Semi-annual cycle. Amplitude and phase distributions for semi-annual periodicity are shown at 10 and 100 m (Figs. 4 and 5). Note that the phases vary from 0° to 180°, with 30° corresponding to one month. At the near surface (Fig. 4a), high amplitudes are found in the western and central regions of the Arabian Sea and low values elsewhere. The distribution pattern follows closely the amplitude distributions of both zonal (τ_x) (Figs. 6a, 9a) and meridional (τ_y) (Figs. 7a, 10a) components of wind stress, discussed in the following section. The phase distribution (Fig. 4b) is constant in the region of large amplitude. The distribution at 100 m (Fig. 5a) shows characteristically high amplitudes in the western and eastern parts of the equatorial region (up to 2.4°C), while away from the equator, the amplitudes decrease rapidly. In the phase distribution at 100 m (Fig. 5b); notably, there is a phase change of about 60° between the western and eastern regions of the equator.

iii. Amplitude and phase distribution of wind stress components and curl of the wind stress. Wind stress components τ_x and τ_y that are obtained from the data set of Hellerman and Rosenstein (1983) and the computed curl of the wind stress are also subjected to the least square analysis and the results are shown in Figures 6–11. The notable features are the intensities of annual and semi-annual signals in both τ_x (Figs. 6a and 9a) and τ_y (Figs. 7a and 10a) in the western part of the northern Indian Ocean. In the equatorial region, the amplitudes are in general low. However, in the western part of the equatorial region, the semi-annual signal of τ_x is stronger than that of τ_y.

Annual cycle of the curl of the wind stress shows a maximum in the central Arabian Sea (Fig. 8a), with the peak occurring during August in the western side. Semi-annual amplitudes of the curl of the wind stress (Fig. 11a) are relatively weaker than the annual ones.

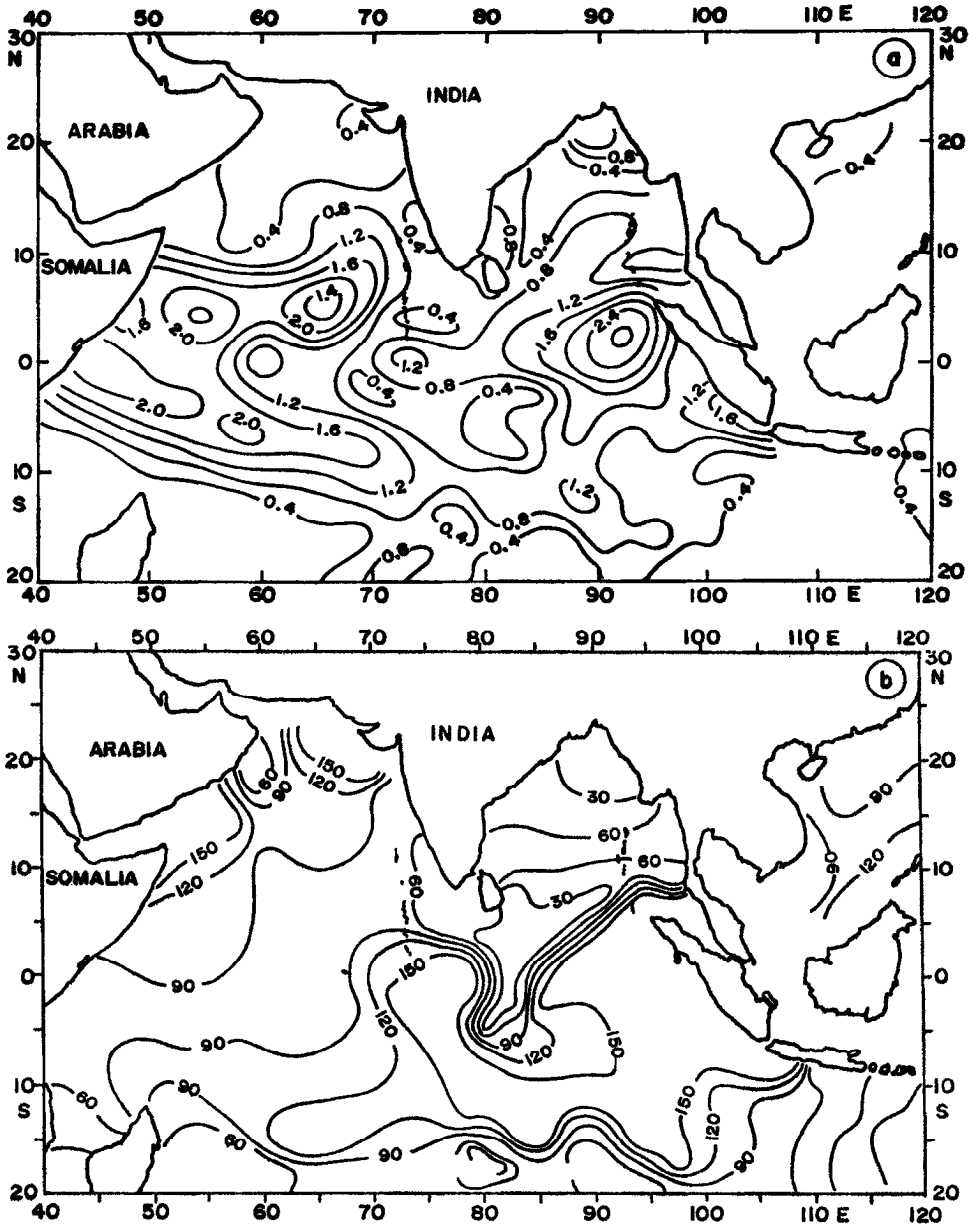

Figure 5. The distribution of (a) amplitude (°C) and (b) phase (deg.) of the seasonal cycle of temperature at 100 m for the semi-annual periodicity. Note that the phase values range from 0 to 180 degrees.

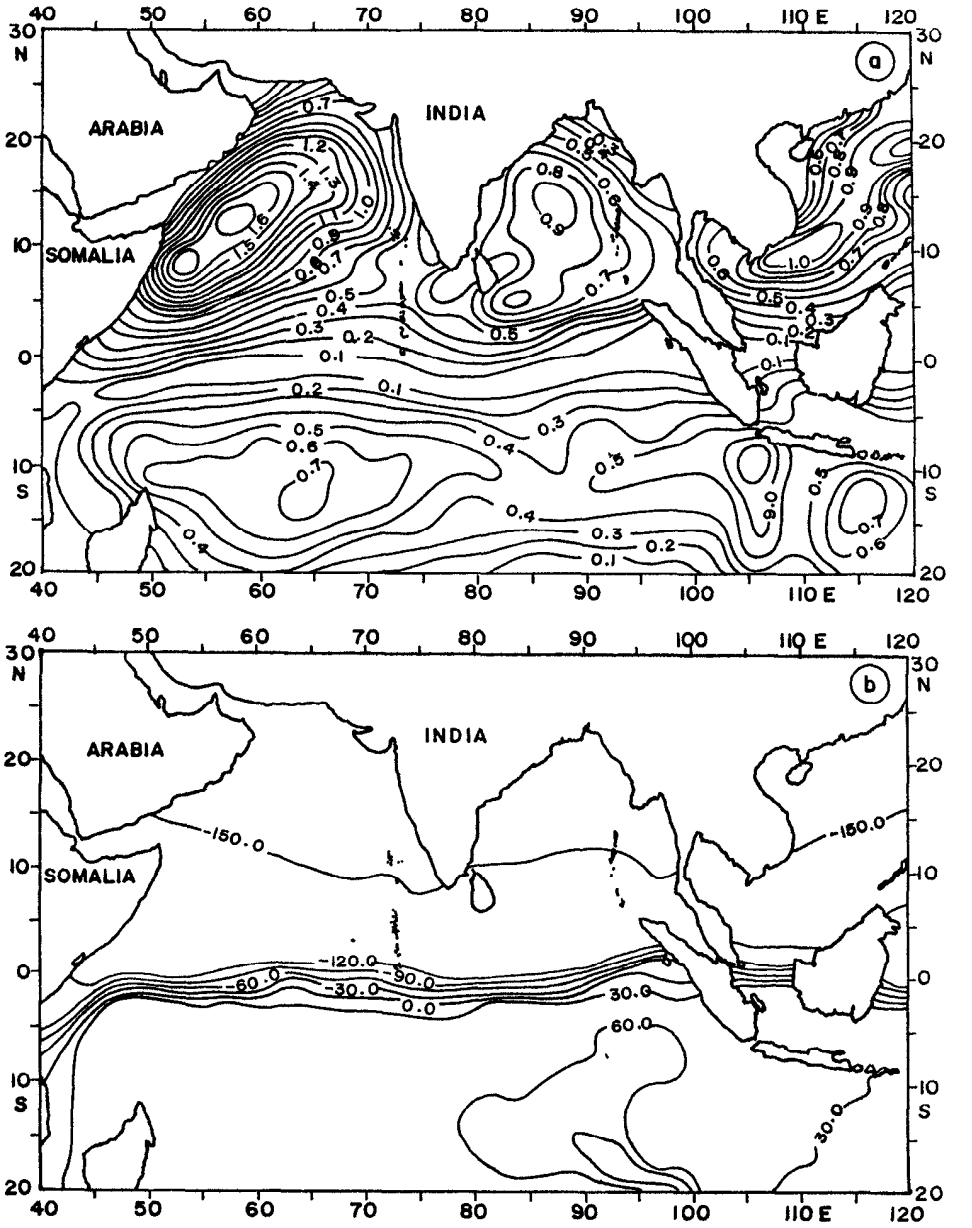

Figure 6. The distribution of (a) amplitude (dynes cm^{-2}) and (b) phase (deg.) of the seasonal cycle of zonal component of wind stress for annual periodicity. Note that the phase values range from −180 to 180 degrees with 0 degree corresponding to the middle of January.

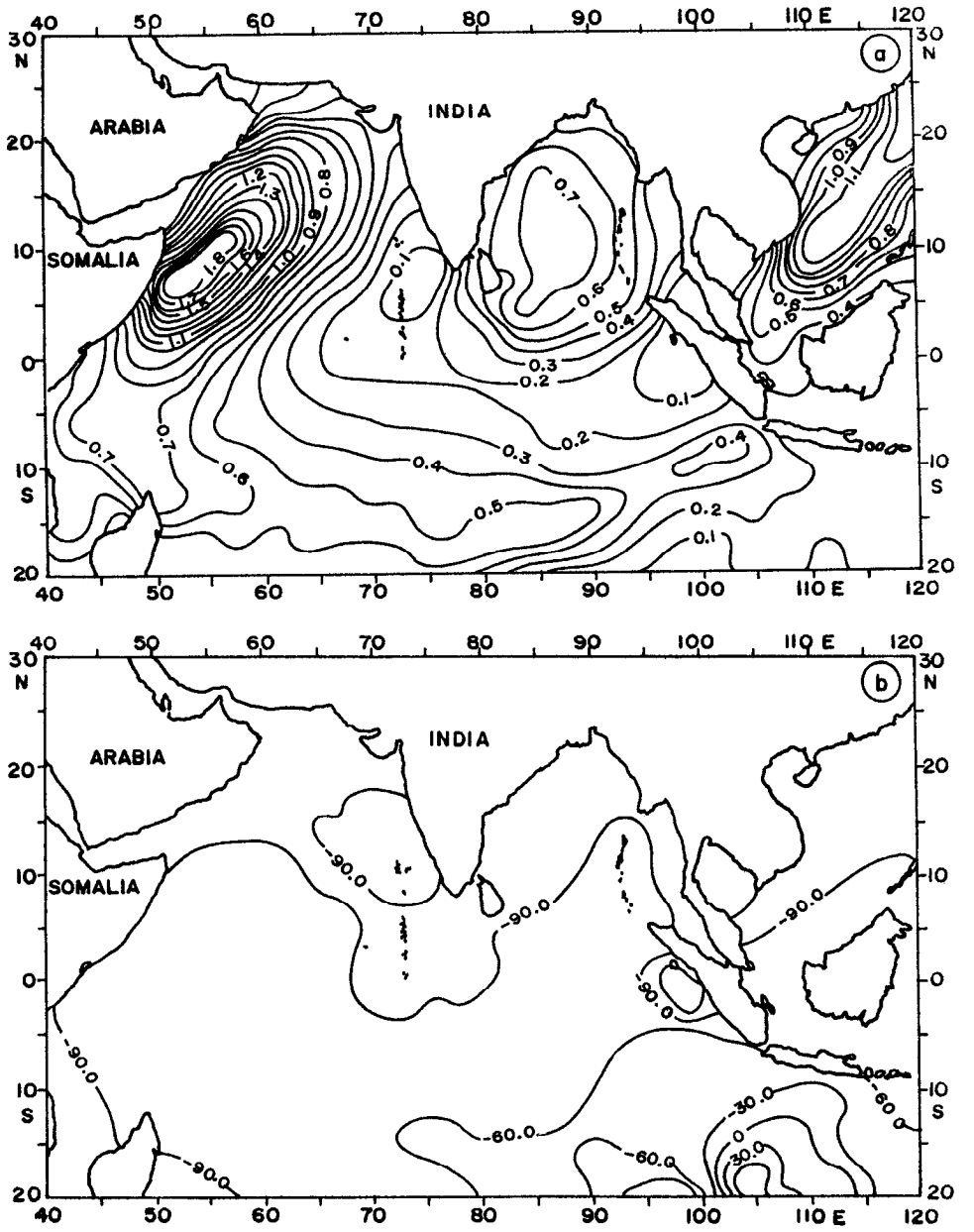

Figure 7. The distribution of (a) amplitude (dynes cm^{-2}) and (b) phase (deg.) of the seasonal cycle of meridional component of wind stress for annual periodicity. Note that the phase values range from −180 to 180 degrees with 0 degree corresponding to the middle of January.

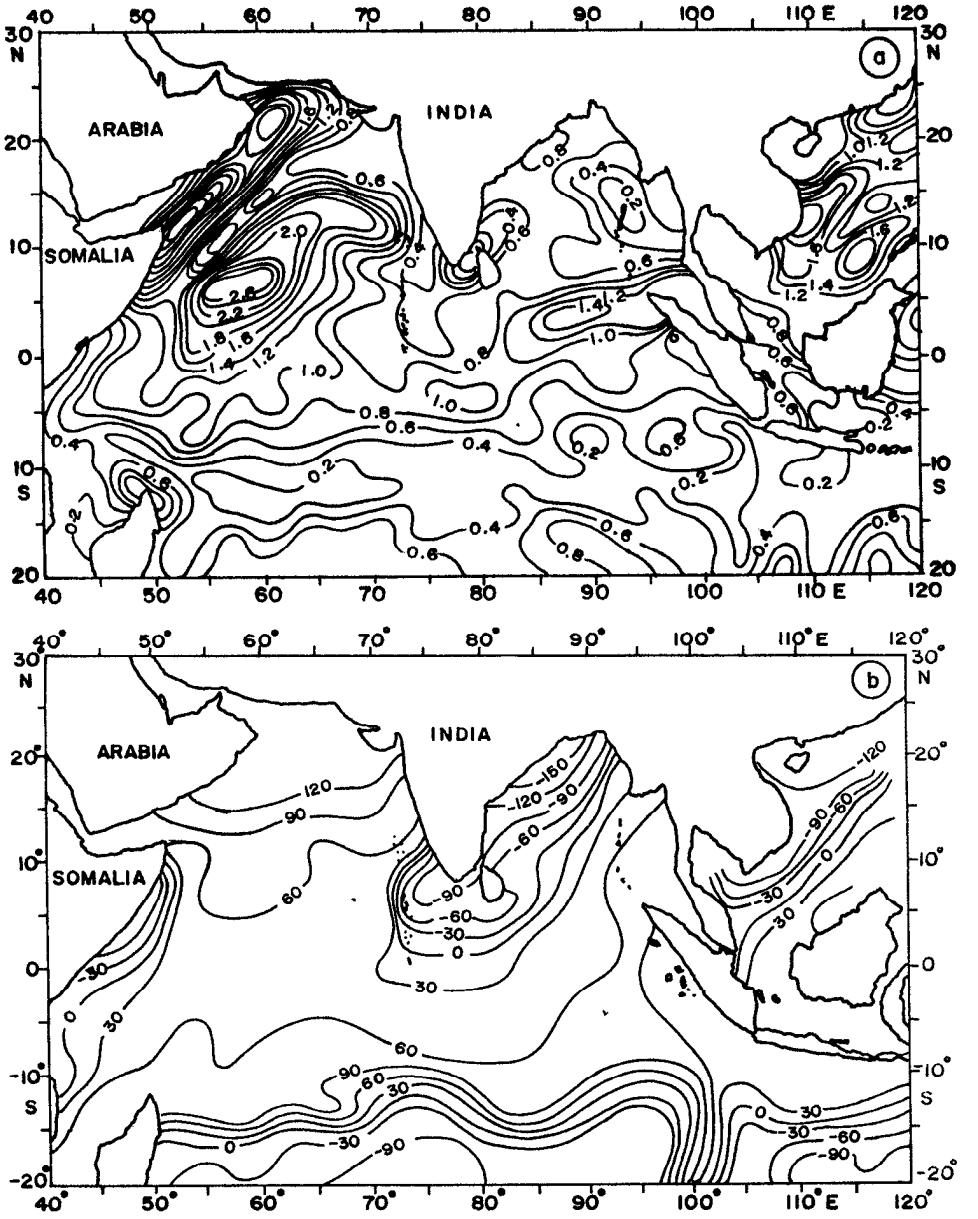

Figure 8. The distribution of (a) amplitude (dynes $cm^{-2} \times 10^{-8}$) and (b) phase (deg.) of the seasonal cycle of curl of wind stress for annual periodicity. Note that the phase values range from −180 to 180 degrees with 0 degree corresponding to the middle of January.

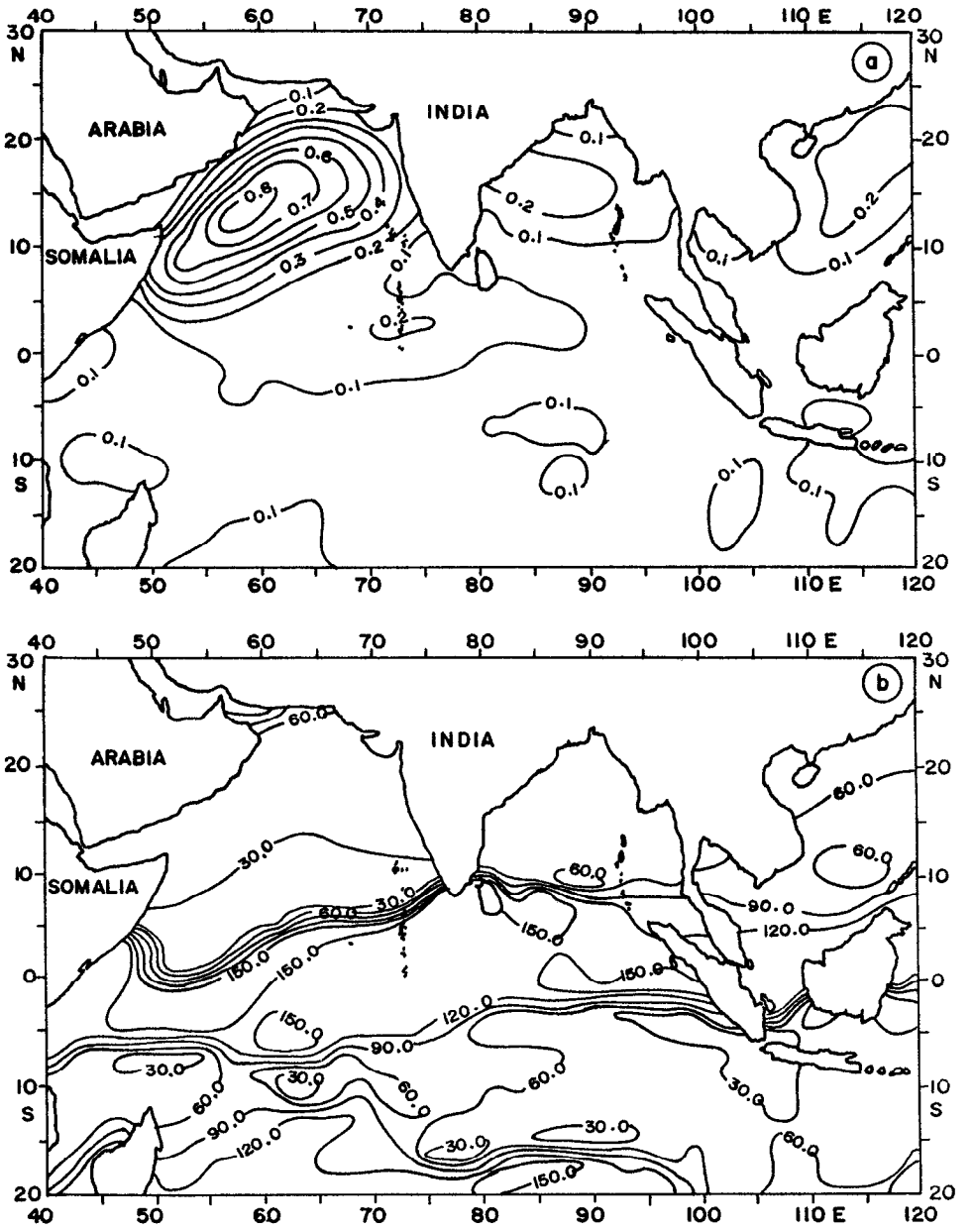

Figure 9. The distribution of (a) amplitude (dynes cm^{-2}) and (b) phase (deg.) of the seasonal cycle of zonal component of wind stress for semi-annual periodicity. Note that the phase values range from 0 to 180 degrees.

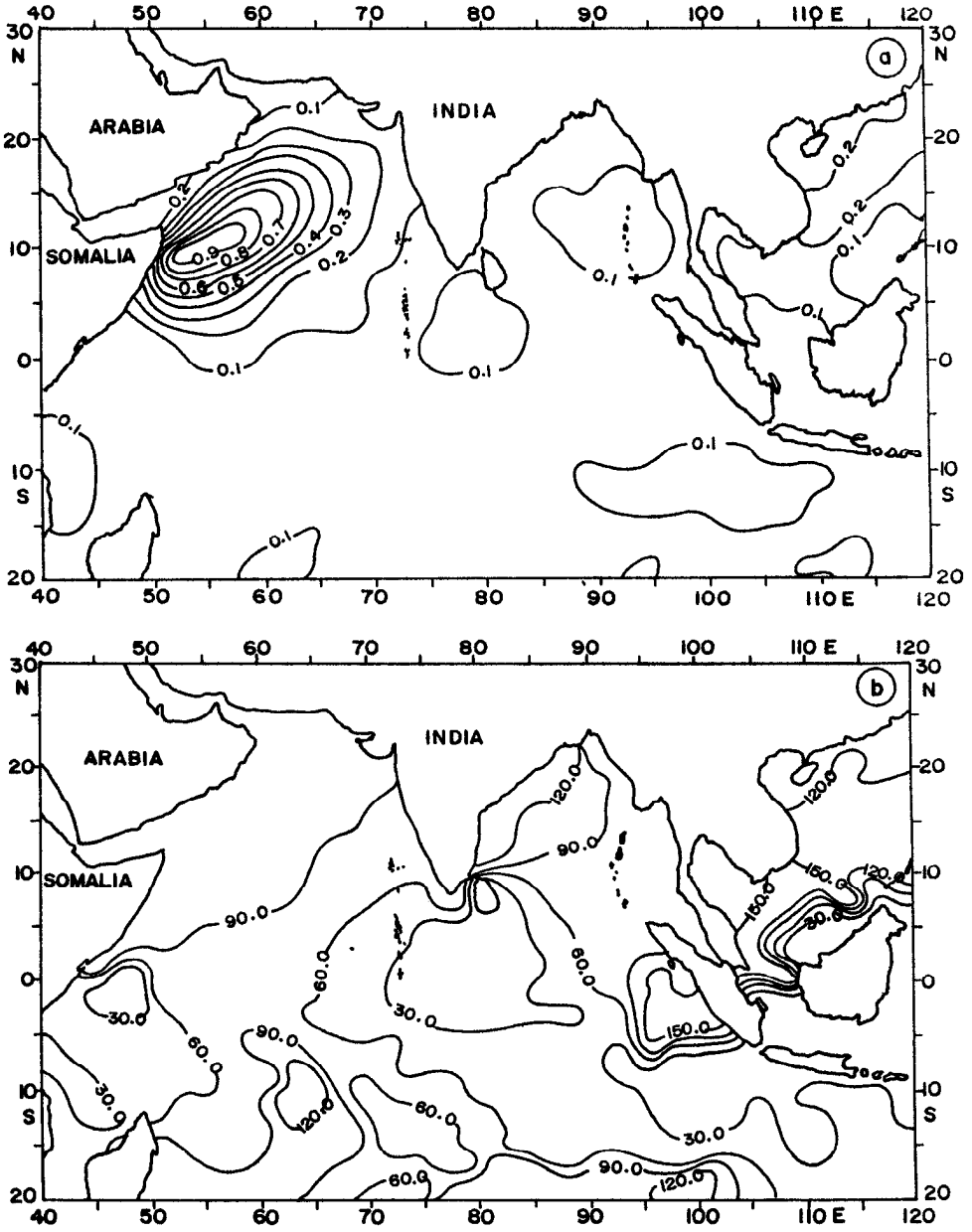

Figure 10. The distribution of (a) amplitude (dynes cm^{-2}) and (b) phase (deg.) of the seasonal cycle of meridional component of wind stress for semi-annual periodicity. Note that the phase values range from 0 to 180 degrees.

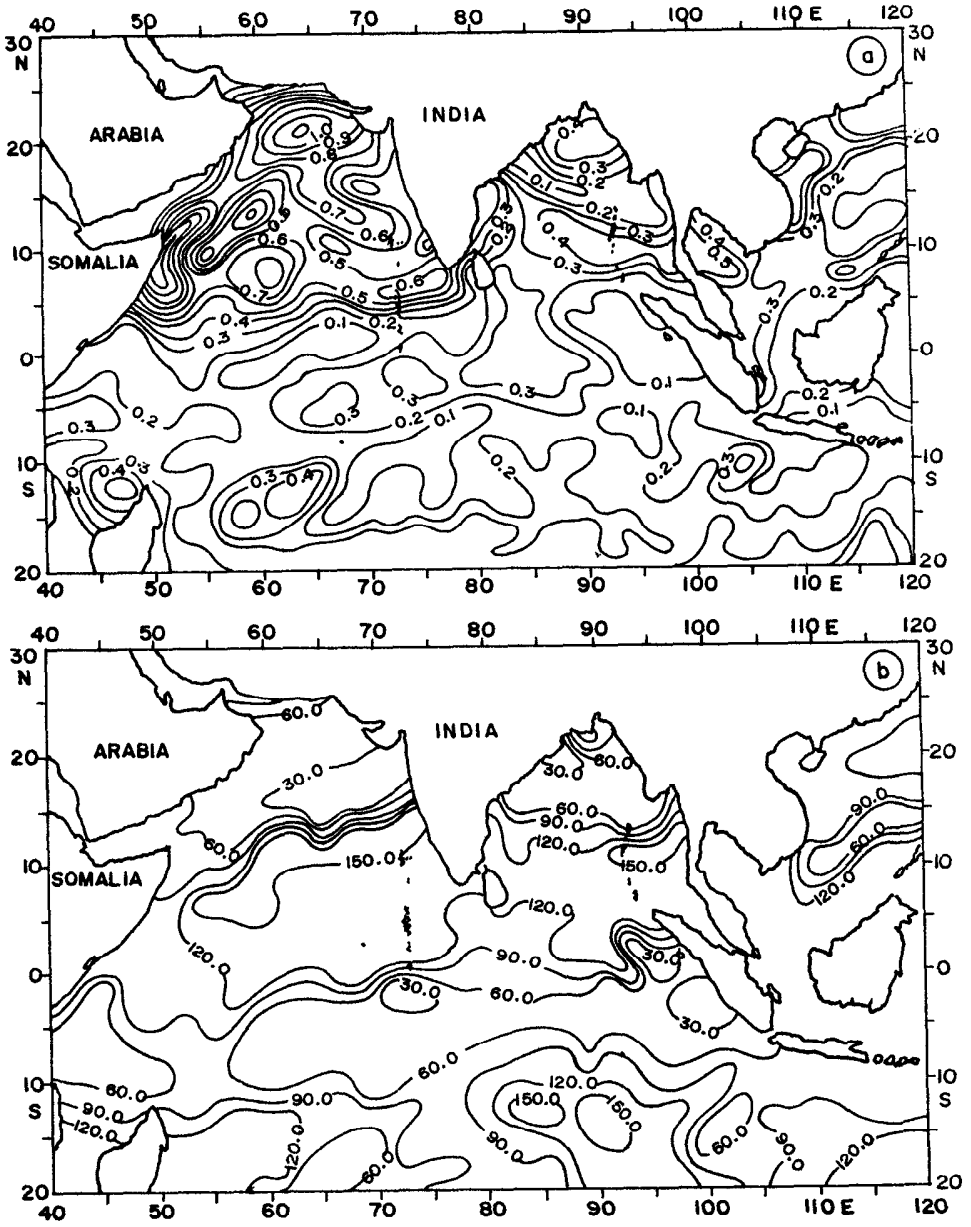

Figure 11. The distribution of (a) amplitude (dynes $cm^{-2} \times 10^{-8}$) and (b) phase (deg.) of the seasonal cycle of curl of wind stress for semi-annual periodicity. Note that the phase values range from 0 to 180 degrees.

b. Depth of 20°C isotherm

In the Indian Ocean, 20°C isotherm is approximately in the midthermocline and oscillations in the thermocline are studied based on the time-longitude plots of the depth of the 20°C isotherm for different latitude sections. (Fig. 12a–f).

The time-longitude plots in the equatorial belt along 0.5S (Fig. 12a), 5.5N (Fig. 12b) and 5.5S (Fig. 12c) show the presence of semi-annual periodicities. Figure 12a indicates that the 20°C isotherm is shallow during May–June on the western side, while greatest depth is found on the eastern side. Similarly, during the month of October a similar feature is noticed. During the transition of monsoons (i.e., in May and October), the winds are westerly near the equator, which generate an eastward jet in the ocean (Wyrtki, 1973). During this time, thermocline is raised in the western side, while it gets depressed in the eastern side. Thus, semi-annual variability in τ_x is reflected in the variability in the thermocline as well.

Farther north, along 10.5N and 15.5N (Fig. 12d, e), the six month periodicities seen in the equatorial region are no longer present. The sloping isolines in these figures indicate westward propagation in the Bay of Bengal and the eastern Arabian Sea. Along 10.5N (Fig. 12d), sloping isolines from the west coast of India (76E) over a distance of about 11° in the zonal direction and over a period of six months give a phase speed of 7.80 cm s^{-1}. Similarly, along 15.5N (Fig. 12e), the corresponding phase speed is 5.2 cm s^{-1}. These values correspond well with those obtained for the Bay of Bengal (8 cm s^{-1} along 12.5N and 4.8 cm s^{-1} along 17.5N) by Prasanna Kumar and Unnikrishnan (1995), which were found to be consistent with theory. These phase speeds are lower, however, consistent with the values obtained from sea surface height (SSH) anomaly derived from Topex/Poseidon altimeter, which are found to be 16.9 and 12.5 cm s^{-1} in the Arabian Sea and the Bay of Bengal respectively for the first baroclinic mode of Rossby waves along 10N (Prasanna Kumar *et al.*, 1996).

There is a broad high between 55 and 70E between June and October (Fig. 12d) associated with large-scale sinking in the central Arabian Sea nearly coinciding with the maxima of wind stress curl (Fig. 8a). There are two elongated lows, persisting for a long time along the coast of Somalia and the west coast of India, the former persisting from May till October, while the latter is present between August and October. These are associated with intense upwelling along the Somali and Arabian coasts and to a lesser extent along the Indian coast. The low found along the west coast of India at 15.5N (Fig. 12e) occurs later than that at 10.5N, while the low found along the Arabian coast becomes broader at 15.5N as compared to that along the Somali coast at 10.5N.

4. Discussion

a. Near-surface variability

The amplitudes for the annual period for the temperature in the near surface (i.e., at 10 m (Fig. 1a)) shows low values (≅0.5°C) in the equatorial region, gradually increasing and reaching to 2.5°C near 20S and 20N. However, in the Somali region, both annual and

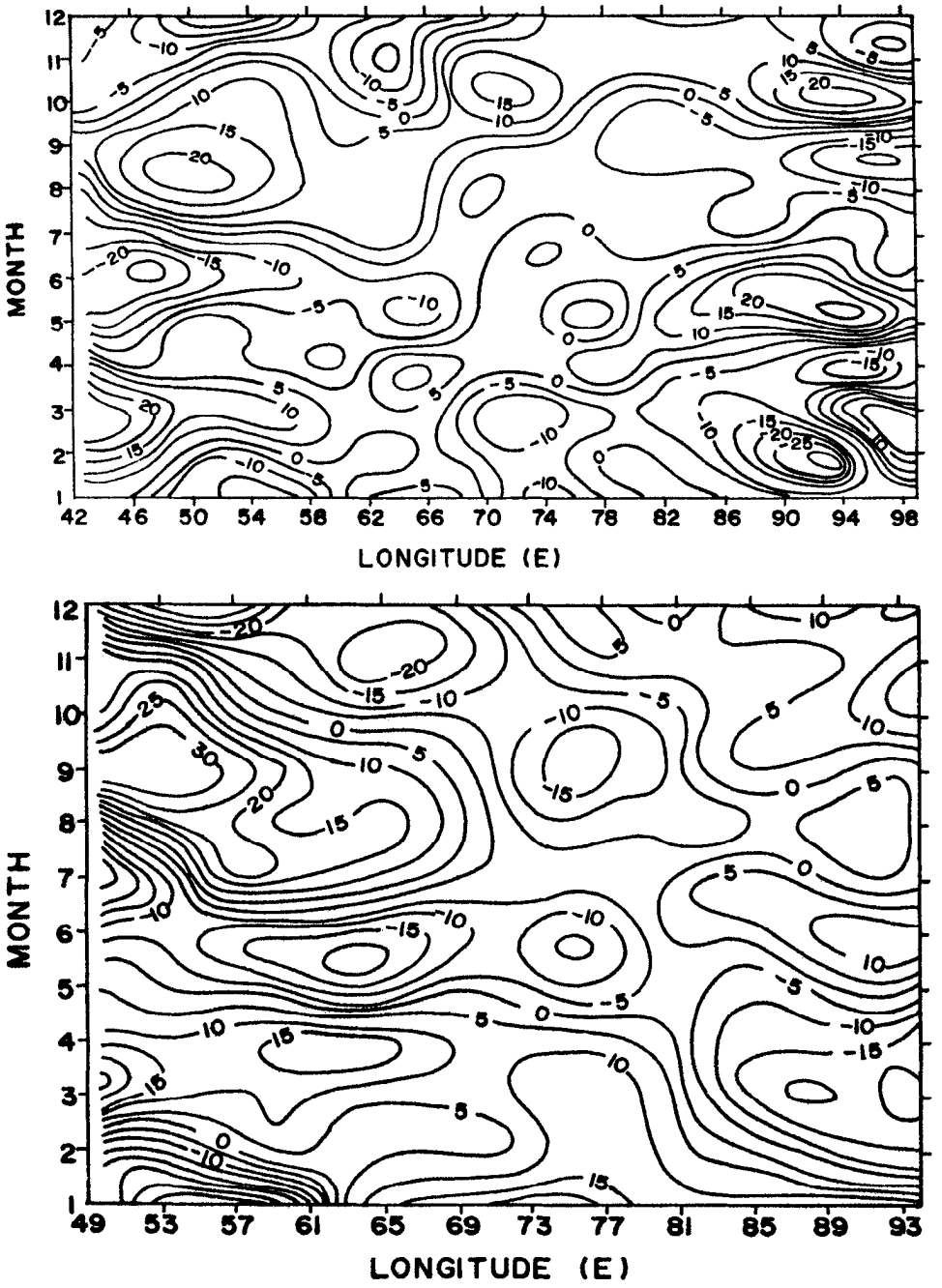

Figure 12. Time-longitude plots of depth (m) of 20°C isotherm along (a) 0.5S, (b) 5.5N, (c) 5.5S, (d) 10.5N, (e) 15.5N and (f) 10.5S. Note that in Figure 12a, time mean is removed while in Figure 12b–f, zonal mean and time mean are removed.

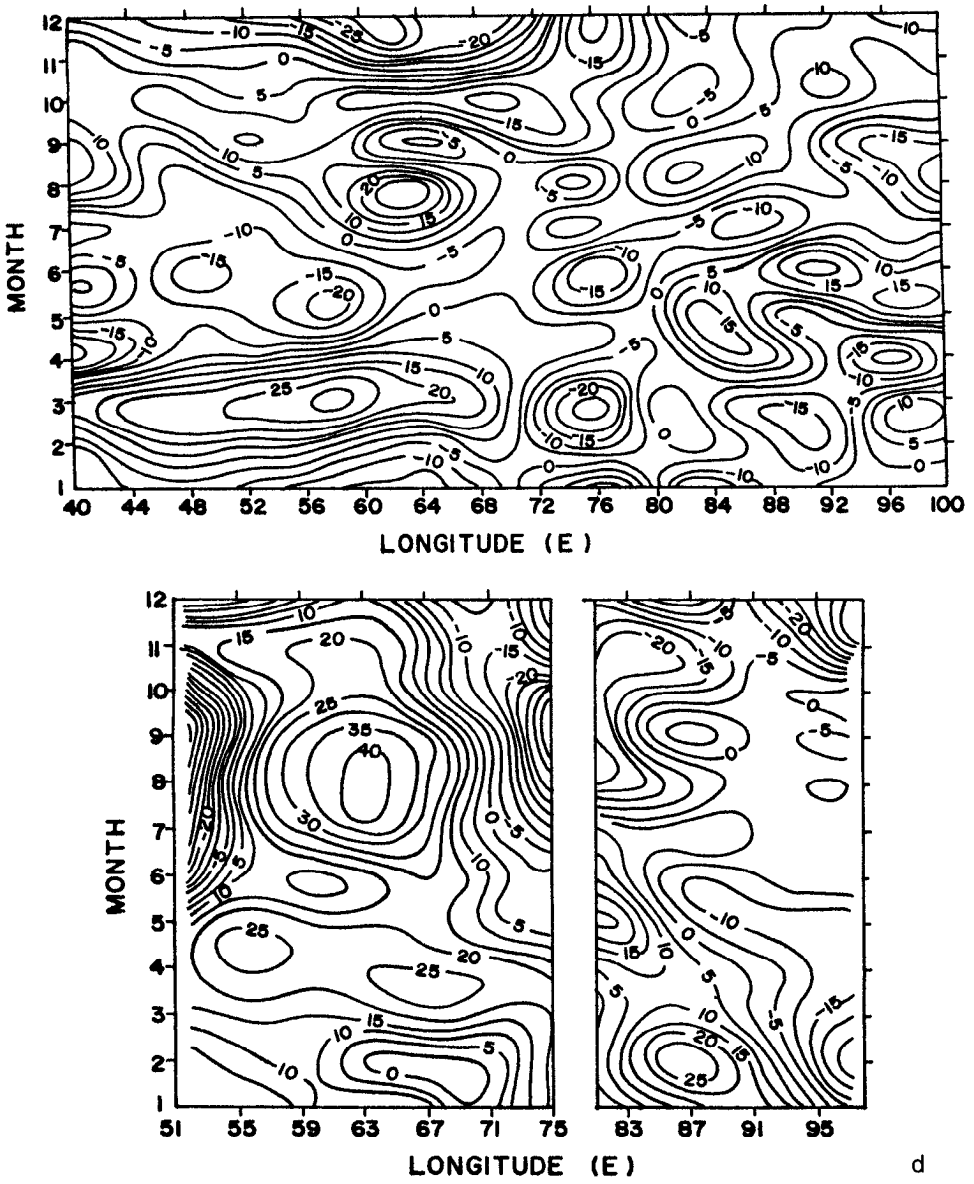

Figure 12. (Continued)

semi-annual amplitudes are high. The pattern is similar to the amplitude distribution charts of SST for the North Pacific (Wyrtki, 1965), where the amplitudes are as low as 0.5°C near the equator, about 2°C near 20N and reach 4°C near 30N, except in the upwelling regions. In the Indian Ocean, ocean-atmosphere exchange rates are low near the equator which increase gradually to the subtropics on both the hemispheres (Ramesh Kumar and Prasad,

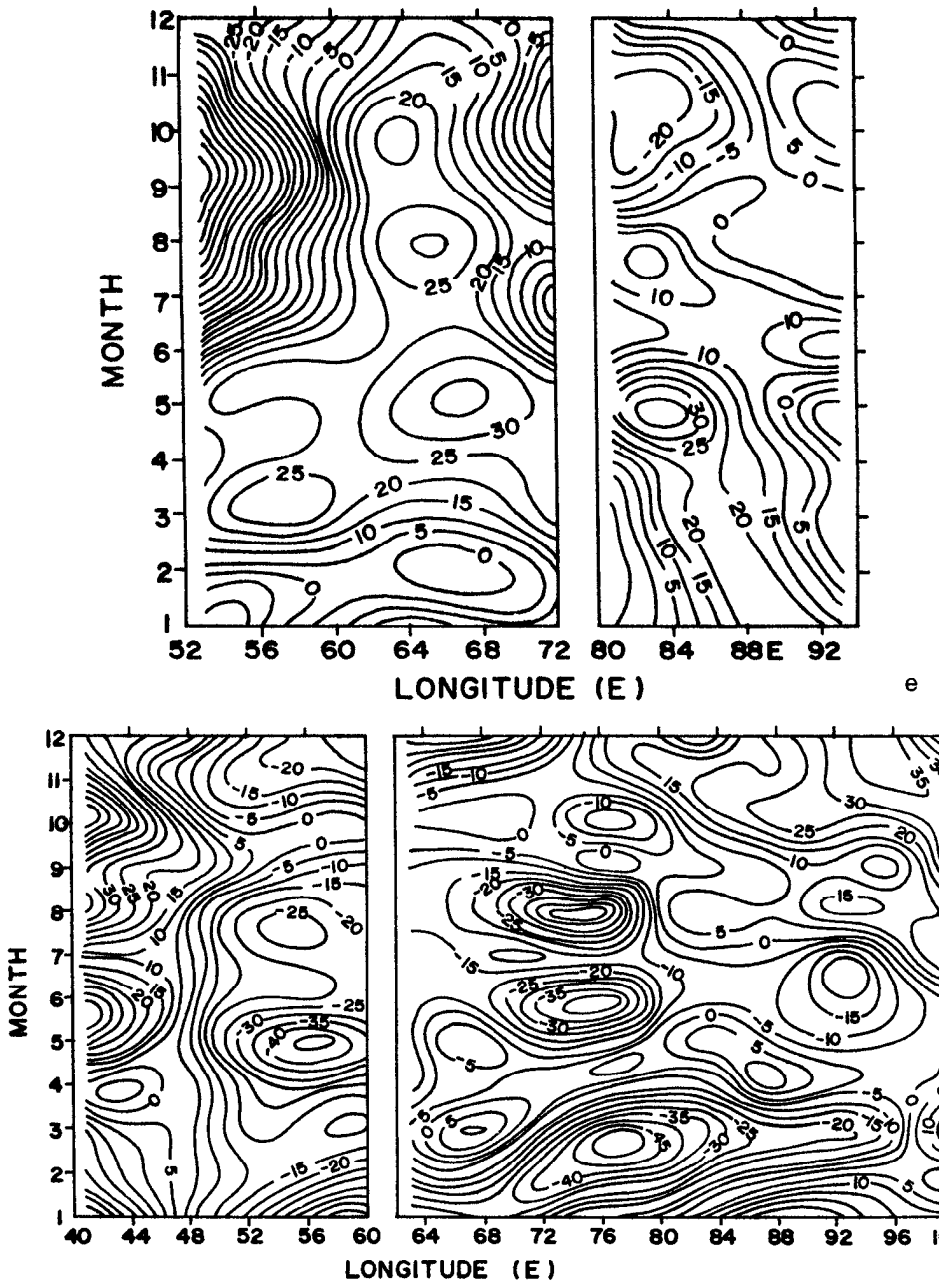

Figure 12. (Continued)

1996). In the Pacific, however, high amplitudes are found in the upwelling regions. In the Indian Ocean also, high amplitudes are found in the upwelling region off Somali. In the semi-annual distribution, amplitudes are significant only in the western region of the Arabian Sea, where both τ_x and τ_y have high values of semi-annual periodicity. One could reasonably assume that the variability in the near surface follows a general pattern found elsewhere, as in the North Pacific, except near the Somali region, where it is influenced by wind.

b. Subsurface variability

i. Semi-annual vs. annual periodicities. In the subsurface, amplitudes obtained for annual and semi-annual periodicities are found to be maximum at 100 m depth. Their distribution shows that semi-annual periodicities dominate in the equatorial region. The time-longitude plots of 20°C isotherm also show the presence of semi-annual periodicities in the equatorial region between 5N and 5S (Fig. 12a–c). Luyten and Roemmich (1982), using the current meter analysis showed the significance of semi-annual period in the region between 47 and 59E, very near the equator. Knox (1976), found that the eastward current extending into the thermocline was in phase with the wind. Clarke and Liu (1993) using sea level analysis showed the significance of semi-annual periodicity at the eastern part of the equatorial Indian Ocean. Gent *et al.* (1983) showed that semi-annual amplitudes of the zonal component of wind stress is stronger than the annual amplitudes in the equatorial Indian Ocean. The semi-annual variability in the zonal component of the wind stress generates eastward-propagating Kelvin waves and nondispersive Rossby waves in the subsurface.

The semi-annual phase lag at 100 m depth between the western and eastern parts of the equator (≅60 degrees, Fig. 5b) corresponds to about two months. This speed is weaker than the theoretical speed of equatorial Kelvin waves, which according to $(g'H)^{1/2}$, is about 2.4 m s^{-1}, giving a time scale of about 32 days to travel from 40E to 100E. However, the SSH calculations mentioned earlier give a phase speed of about 1.25 m s^{-1}, corresponding to a time scale of 61 days over the same zonal distance. Clarke and Liu (1993) found that the first and second mode Kelvin waves in the equatorial Indian Ocean have phase speeds of 2.66 and 1.60 m s^{-1} respectively and they showed that the Indian Ocean has a semi-annual basin mode for the second vertical mode.

ii. Remote vs. local forcing. We now try to relate the observed changes in the thickness of 20°C isotherm to the dynamics of the region. In order to understand the relative importance of local forcing and remote forcing to the seasonal variability, we apply the following equation (McCreary, 1977)

$$h_t - \frac{\beta g' h_o}{f^2} h_x = -\left(\frac{\tau_y}{f}\right)_x + \left(\frac{\tau_x}{f}\right)_y$$

where h is the thickness of the upper layer; h_o, the mean thickness of the upper layer; g' is the reduced gravity; f, the Coriolis parameter; x and y are the eastward and northward directions. τ_x and τ_y are the wind stress components divided by density and β is f_y. The above equation represents the variation of height of the upper layer in a two-layer ocean. It states that there are two processes that determine the vorticity balance, namely, the local Ekman pumping and remote forcing by westward propagating nondispersive Rossby waves. The model, valid for extra equatorial regions, can be applied for large spatial scales of the order of 1000 km and time scales exceeding three to four months.

Ekman pumping velocities are computed using the wind stress data of Hellerman and Rosenstein (1983) and the time-longitude plots of these velocities are made along 5 and 9N (Fig. 13a and b).

Along 5N (Fig. 13a), Ekman pumping velocity distribution shows a narrow region of positive values close to the western boundary, east of which there is a large region (55–70E) of negative values occurring during June to November. The values are positive near the eastern boundary also. In the Bay of Bengal, however, Ekman pumping velocities are low.

It could be inferred that the large high found in the depth of 20°C isotherm between 55E and 70E (Fig. 12d) during June and November corresponds to high negative velocities of Ekman pumping associated with sinking. The two lows seen in the western region of the Arabian Sea, along the coasts of Somalia and Arabia during May to October (Fig. 12d, e) result from upwelling. Thus the local winds control the dynamics in the western and central Arabian Sea. Bauer *et al.* (1991) found that the negative wind stress curl southwest of the Findlater jet causes open ocean downwelling, while the positive curl in the northeast causes upwelling. Obviously, the intense upwelling along the Arabian coast is augmented by this process.

In the Bay of Bengal and the eastern Arabian Sea, sloping isolines along 10.5N and 15.5N (Fig. 12d, e) indicate signatures of westward propagation. In these regions, the computed Ekman pumping velocities are low suggesting the dominance of remote forcing over local effects.

The high amplitudes (Fig. 2a) off the southwest coast of India is a remarkable feature. The fact that seasonal signatures of τ_x and τ_y and curl of the wind stress are low in this region suggests that this phenomenon is remotely forced. McCreary *et al.* (1993), through model studies, found that Rossby waves are radiated from the southern tip of India. A similar evidence is reported in Antony and Unnikrishnan (1992). They found that the upwelling front found along the west coast of India during September has an offshore spread in the southern side. Thus, the seasonal variabilities in the Arabian Sea are associated with local forcing by the wind stress and curl of the wind stress in the western coast (Somalia), Ekman pumping in the central region, and remote forcing in the eastern side.

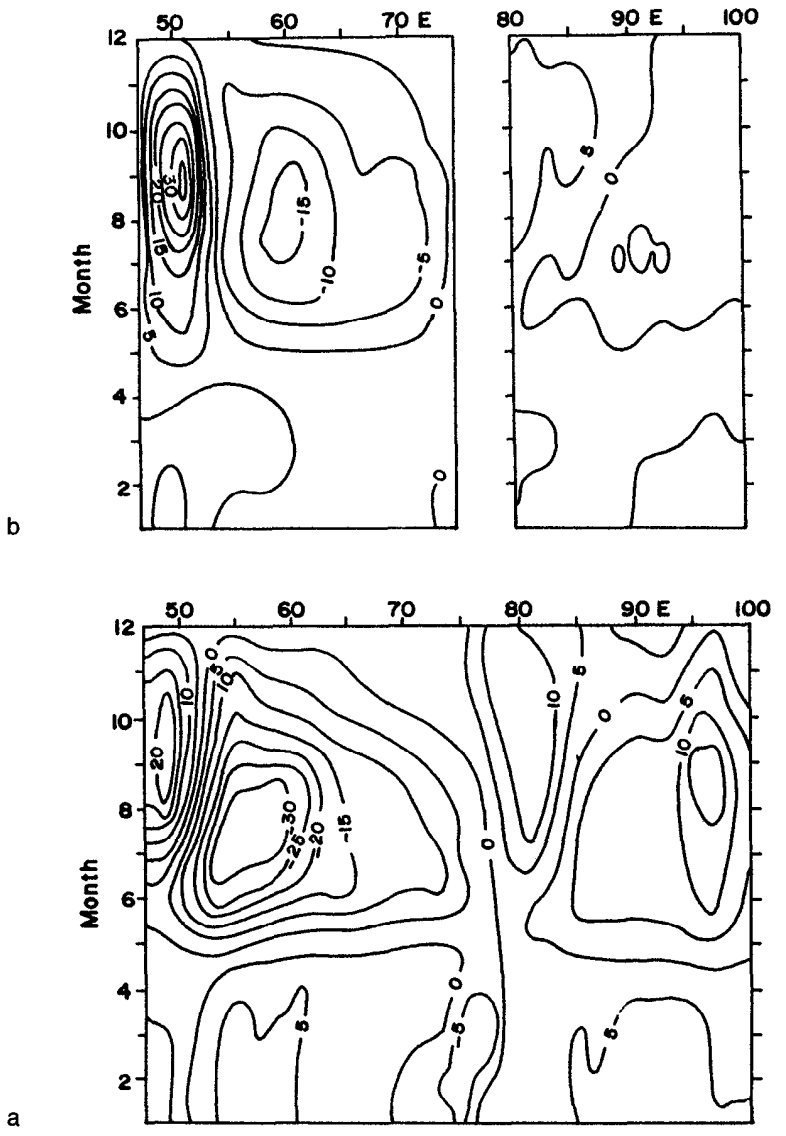

Figure 13. Ekman pumping velocities along (a) 5N and (b) 9N. The units are in 10^{-8} cm s^{-1}. Negative values indicate downwelling.

Acknowledgments. The authors thank the Director, National Institute of Oceanography, for providing the facilities and encouragement. We are grateful to the anonymous referees for their valuable suggestions. This is NIO contribution no. 2501.

REFERENCES

Antony, M. K. and A. S. Unnikrishnan. 1992. On an upwelling front, propagation of upwelling and vertical velocity in the eastern Arabian Sea during monsoon, 1987. Proc. PORSEC-'92, Okinawa, Japan, 527–532.

Bruce, J. D., R. Quadfasel and J. C. Swallow. 1980. Somali eddy formation during the commencement of the southwest monsoon. J. Geophys. Res., *85,* 6654–6660.

Bauer, S., G. L. Hitchcock and D. B. Olson. 1991. Influence of monsoonally forced Ekman dynamics upon surface layer depth and plankton biomass distribution in the Arabian Sea. Deep-Sea Res., *38,* 531–553.

Clarke, A. J. and X. Liu. 1993. Observations and dynamics of semi-annual and annual sea levels near the eastern equatorial Indian Ocean Boundary. J. Phys. Oceanogr., *23,* 386–399.

Cutler, A. N. and J. C. Swallow. 1984. Surface currents of Indian Ocean. Institute of Oceanographic Sciences Report 187, 8 pp. & 36 charts.

Gent, P. R., K. O'Neill and M. A. Cane. 1983. A model of the semi-annual oscillation in the equatorial Indian Ocean. J. Phys. Oceanogr., *13,* 2148–2160.

Grundlingh, M. L. 1985. An intense cyclonic eddy east of the Mozambique Ridge., J. Geophys. Res., *90,* 7163–7167.

Hellerman, S. and M. Rosenstein. 1983. Normal monthly wind stress curl over the world ocean with error estimates. J. Phys. Oceanogr., *13,* 1093–1104.

Knox, R. D. 1976. On a long series of measurements of Indian Ocean equatorial currents near Addu Atoll. Deep-Sea Res., *23,* 211–222.

Levitus, S. 1982. Climatological Atlas of the world ocean. NOAA professional paper No. 13, U.S. Gov. Printing Office, Washington D.C., 173 pp.

Lutjeharms, J. R. E. 1981. Characteristics of the currents east and south of Madagascar. Deep-Sea Res., *28,* 879–899.

Luyten, J. R. and D. H. Roemmich. 1982. Equatorial currents at semi-annual period in the Indian Ocean. J. Phys. Oceanogr., *12,* 406–413.

McCreary, J. P. 1977. Eastern ocean response to changing wind system. Ph.D. dissertation, Univ. of California, San Diego, 156 pp.

McCreary, J. P., P. K. Kundu and R. L. Molinari. 1993. A numerical investigation of dynamics, thermodynamics and mixed layer processes in the Indian Ocean. Prog. Oceanogr., *31,* 181–244.

Prasanna Kumar, S., S. M. Snaith, P. G. Challenor and T. H. Guymer. 1996. Large scale sea surface height variations of the Indian Ocean inferred from Topex/Poseidon Altimeter. Technical Report. Southampton Oceanography Centre, U.K., 63 pp.

Prasanna Kumar, S. and A. S. Unnikrishnan. 1995. The seasonal cycle of temperature and associated wave phenomena in the Bay of Bengal. J. Geophys. Res., *100,* 13585–13593.

Quadfasel, D. R. and F. Schott. 1982. Water-mass distributions at intermediate layers off the Somali coast during the onset of the southwest monsoon 1979. J. Phys. Oceanogr., *12,* 1358–1372.

—— 1983. Southward subsurface flow below the Somali current. J. Geophys. Res., *88,* 5973–5979.

Ramesh Kumar, M. R. and T. G. Prasad. 1996. Annual and Interannual variation of precipitation over the tropical Indian Ocean. J. Geophys. Res., (submitted).

Rao, R. R., R. L. Molinari and J. F. Festa. 1989. Evolution of the Climatological Near-Surface Thermal Structure of the Tropical Indian Ocean 1. Description of mean monthly mixed layer depth

and Sea Surface Temperature, Surface Current and Meterological Fields. J. Geophys. Res., *94,* 10801–10815.

Schott, F., J. C. Swallow and M. Fieux. 1990. The Somali current at the equator: Annual cycle of the currents and transports in the upper 1000 m and connection to neighboring latitudes. Deep-Sea Res., *37,* 1825–1848.

Swallow, J. C., M. Fieux and F. Schott. 1988. The boundary current east and south of Madagascar. Part I: Geostrophic currents and transports. J. Geophys. Res., *93,* 4951–4962.

Wyrtki, K. 1965. The annual and semi-annual variation of sea surface temperature in the North Pacific Ocean. Limnol. Oceanogr., *10,* 307–313.

—— 1971. Oceanographic atlas of the International Indian Ocean Expedition. National Science Foundation, Washington D.C., 531 pp.

—— 1973. An equatorial jet in the Indian Ocean. Science, *181,* 262–264.

Received: *24 August, 1995;* revised: *9 July, 1996.*